Pergamon

Solid State Communications, Vol. 107, No. 11, pp. 607–616, 1998

0038–1098/98 $ - see front matter

PII: S0038–1098(98)00209-9

# ONE-DIMENSIONAL NANOSTRUCTURES: CHEMISTRY, PHYSICS & APPLICATIONS

Charles M. Lieber

Harvard University, Cambridge, MA 01238, U.S.A.

Nanometer scale structures represent an intellectually challenging and rapidly expanding area of research that crosses the borders between many areas of the physical sciences and engineering. In this review, results, drawn primarily from the author's laboratory, and addressing the rational growth, physical properties and applications of 1D nanostructures will be discussed. In addition, present and future challenges in this broad area of research are outlined. © 1998 Elsevier Science Ltd. All rights reserved

Keywords: A. nanostructures, B. crystal growth, C. scanning tunnelling microscopy, D. electronic band structure, D. mechanical properties.

## 1. INTRODUCTION

Nanometer scale structures represent an exciting, intellectually challenging and rapidly expanding area of research that crosses the borders between many areas of the physical sciences and engineering [1–5]. Nanostructures can be defined as systems in which at least one dimension is $\leq 100$ nm; that is, reducing 1, 2 or 3 dimensions (D) of a bulk material to the nanometer scale produces nanometer thick 2D layers, 1D nanowires, or 0D nanoclusters, respectively. Interest in nanometer scale structures has been driven by fascinating questions and the potential to impact basic science and technology. Two questions at the heart of basic chemistry and physics research are (i) how can nanostructures that have controlled dimensionality and size be rationally synthesized or fabricated and (ii) what are the intrinsic and potentially unique physical properties of nanostructures? In this overview, we focus on these questions in the context of 1D nanostructures: nanowires and nanotubes.

Our focus on nanometer scale wires is motivated by basic scientific and technology questions. How can atoms or other building blocks be assembled rationally into structures with nanometer size diameters but much longer lengths? There are now relatively well-developed methods for the synthesis of 0D nanoclusters via arrested precipitation [6] and the growth of 2D layers using molecular beam epitaxy, although general methods for the growth of 1D structures with diameters $< 10$ nm have not been available. In addition, 1D structures with nanometer diameters, such as nanowires and nanotubes, have great potential for testing and understanding fundamental concepts about the roles of dimensionality and size on physical properties. For example, 1D systems should exhibit density of states singularities, can have energetically discrete molecular states extending over large linear distances and may show more exotic phenomena, such as spin-charge separation predicted for a Luttinger liquid [7, 8]. There are also many applications where 1D nanostructures could be exploited, including (i) nanoelectronics, (ii) functional, nanostructured materials and (iii) novel probe microscopy tips. To realize these and other exciting uses of 1D nanostructures will, however, require an understanding of the fundamental chemistry and physics questions raised above. Our progress addressing these challenges is described below.

## 2. SYNTHESIS OF NANOWIRES

How can atoms or other building blocks be rationally assembled into structures with nanometer size diameters but much longer lengths? Answering this question is central to the preparation of 1D nanostructures, and correspondingly, researchers have pursued several strategies to synthesize nanotubes and nanowires [5, 9–13]. For example, multiwall carbon nanotubes have been prepared via the condensation of hot carbon plasmas [9]. The growth mechanism producing these 1D nanostructures is, however, specific to the tubular structures

of $sp^2$-bonded carbon and isostructural hexagonal boron nitride. It is also possible to favor the formation of singlewall carbon nanotubes from carbon plasmas by adding certain metals [10]. These metals presumably function as catalysts, although the growth mechanism is not well-defined. In addition, template directed synthesis has been used to prepare 1D nanostructures [5, 11–13]. The nanometer diameter pores in membranes and zeolites have been used to confine the growth of wires [11, 12] and carbon nanotubes have been converted to carbide nanowires [5, 13]. Although a promising and conceptually simple technique, template mediated growth generally produces polycrystalline materials with diameters greater than 10 nm. Hence, it is unclear based on these previous studies whether a general method for the growth of single crystal nanowires with diameters $< 10$ nm exists.

An approach that can yield single crystal wire-like structures is vapor-liquid-solid (VLS) growth [5, 14, 15]. In VLS growth, a liquid metal cluster or catalyst acts as the energetically favored site for vapor-phase reactant adsorption and when supersaturated, the nucleation site for crystallization. Preferential 1D growth occurs in the presence of reactant as long as the catalyst remains liquid. Most previous 1D structures produced by VLS growth have had diameters $> 0.1$ $\mu$m. This relatively large lower size limit, which precludes the study of interesting 1D phenomena, is determined in large part by the minimum diameter liquid metal catalyst that is achievable under the equilibrium conditions typically used for growth [15].

Methods that constrain the catalyst cluster to diameters in the 10 nm size regime could thus enable the growth of nanowires. A straightforward approach to produce such small clusters is laser ablation and condensation, which has been studied extensively in the past to generate nanometer diameter clusters [16]. Nanowire growth can be achieved by laser ablation of the catalyst material in a heated flow tube in which the pressure and temperature are varied (Fig. 1). The background pressure is used to control condensation and cluster size, while the temperature can be varied to maintain the catalyst cluster in the liquid state. Nanowire growth initiates after a laser-generated cluster becomes supersaturated and ceases when the nanowire and attached liquid cluster pass out of the hot-zone of the furnace as shown in Fig. 1. We believe that this approach to growth is quite significant in that it enables *a priori* prediction of reaction conditions (using equilibrium phase diagrams) to prepare single crystal nanowires of virtually any material.

We illustrate this approach with published studies for the synthesis of single crystal Si and Ge nanowires having diameters as small as 6 nm and 3 nm, respectively,

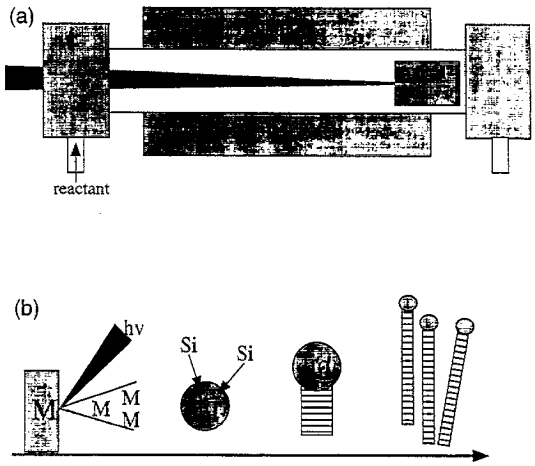


Fig. 1. (a) Schematic of the nanowire growth apparatus. The output from a pulsed laser is focused onto a target located within a quartz tube; the reaction temperature is controlled by a tube furnace. (b) Nanowire growth process. Laser ablation of the metal (M) target creates a dense, hot vapor that condenses into nanoclusters as the metal and Si species cool through collisions with the buffer gas. The furnace temperature is controlled to maintain the metal-Si nanocluster in a liquid state. Nanowire growth begins after the liquid becomes supersaturated in Si and continues as long as the metal-Si nanoclusters remain in a liquid state and Si reactant is available. Growth terminates when the nanowire passes out of the hot reaction zone.

and lengths greater than one micrometer [5, 17]. Consider the synthesis of Si nanowires. The critical catalyst and temperature for nanowire growth can be determined by examining the Si rich region of binary metal-Si phase diagrams; for example, the Si-rich region of the Fe–Si phase diagram exhibits a broad area above 1200°C where $FeSi_x(l) + Si(s)$ coexist. Significantly, transmission electron microscope (TEM) images of the product obtained after laser ablation of a $Si_{0.9}Fe_{0.1}$ target at 1200°C shows primarily wire-like structures with remarkably uniform diameters on the order of 10 nm with lengths $> 1$ $\mu$m and often as large as 30 $\mu$m [Fig. 2(a)]. Electron-induced X-ray fluorescence (EDX) analysis of individual nanowires shows that they contain only Si and O. In addition, the TEM images show that virtually all of the nanowires terminate at one end in nanoclusters having diameters about 1.5 times that of the connected nanowire. The observation of nanocluster spheres at the ends of the nanowires is suggestive of the catalytic growth process.

Higher resolution TEM images recorded on individual nanowires have provided further insight into the structure of these materials [Fig. 2(b) and 2(c)]. First, diffraction contrast images have shown that the nanowires consist of a very uniform diameter crystalline core surrounded by an amorphous coating [Fig. 2(b)]. The nanowires produced

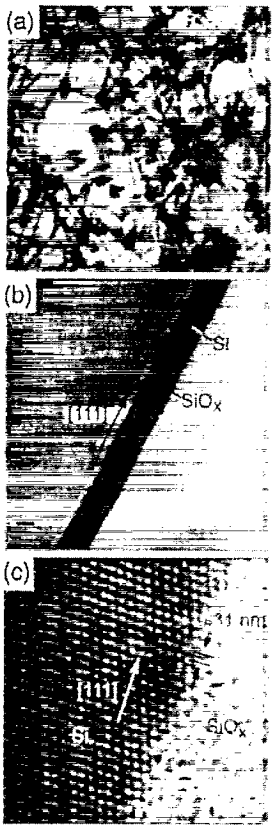


Fig. 2. (a) TEM image of the nanowires produced following ablation of a $Si_{0.9}Fe_{0.1}$ target. The white scale bar corresponds to 100 nm. (b) Diffraction contrast TEM image of a silicon nanowire; crystalline material (the silicon core) appears darker than amorphous material ($SiO_2$ sheath) in this imaging mode. The scale bar corresponds to 10 nm. (c) High-resolution TEM image of the crystalline silicon core and amorphous $SiO_2$ sheath. The (1 1 1) planes (spacing 0.31 nm) are oriented perpendicular to the growth direction (white arrow). Adapted from [17].

at 1200°C grow preferentially along the [1 1 1] direction as shown by convergent beam electron diffraction and lattice-resolved TEM images of the crystalline core [Fig. 2(c)]. Taken together, these data have shown that the nanowires produced using our laser-based method consist of crystalline silicon cores that grow along the [1 1 1] direction and are sheathed by amorphous silicon oxide.

The essential details of our growth mechanism, which were illustrated in Fig. 1, have also been confirmed in our experiments [17]. Quantitative EDX analysis of the clusters at the ends of the nanowires have shown that these nanoclusters have the expected $FeSi_2$ composition. In addition, TEM images of these nanoclusters show atomic planes separated by 0.51 nm and are thus in good agreement with the 0.510 nm distance between (0 0 1) planes in $\beta$-$FeSi_2$. Lastly, the growth of Si nanowires occurs only for temperatures greater than 1150°C using the Fe catalyst. The observation of Si nanowire growth at temperatures below the bulk solidus line at 1207°C is reasonable, because the melting points of nanoclusters are lower than the corresponding bulk solids [18].

The good agreement between our experimental data and growth model suggest that it should be possible to choose rationally new catalysts and growth conditions for nanowire synthesis. To illustrate this point we have examined other binary Si-metal phase diagrams. This analysis shows that, like Si–Fe, Si–Ni and Si–Au have eutectic silicon rich regions with silicon as the primary solid phase. Significantly, laser vaporization of silicon targets containing either Ni or Au, or vaporization of pure Au in the presence of silane, produce Si nanowires that have the same structural characteristics as those described above for the Si–Fe system. In addition, virtually all of the Si nanowires produced using the Ni and Au catalysts terminate in $\beta$-$NiSi_2$ and Au nanoclusters, respectively. It is especially significant from the standpoint of observing interesting physical phenomena that growth using silane and ablated Au clusters can produce single crystal nanowires as small as 3 nm [19]. Au has been used in the past as a VLS catalyst for Si growth, primarily on surfaces [15, 20], although previously a direct growth of single crystal Si nanowires $< 10$ nm diameter had not been achieved.

The experimental data presented for Si nanowire growth provide strong support for the generality of our approach. In addition, we have made a more stringent test by preparing Ge nanowires. Examination of the Ge binary phase diagrams shows that the Ge-rich region of the Ge–Fe diagram is similar to that of the Si–Fe diagram; that is, the phase above 838°C are $FeGe_x(l) + Ge(s)$ and below this temperature are $\beta$-$FeGe_2(s) + Ge(s)$. Hence, the major difference between Ge–Fe and Si–Fe is that the solidus line lies about 400°C lower in the former. Laser ablation of a $Ge_{0.9}Fe_{0.1}$ target at 820°C produced a good yield of wire-like products with diameters between 3 and 9 nm and TEM images have shown that these nanowires are crystalline, have uniform diameters without an amorphous coating and terminate in nanoclusters [17]. EDX analysis has further confirmed that the nanowires consist primarily of Ge and that the nanoclusters have the expected $FeGe_2$ composition.

The above studies illustrate clearly the potential of our approach for the synthesis of crystalline nanowires. In short, a good starting point for the synthesis of nanowires of a specific composition should be an alloy that has an eutectic region with the specific material of interest. The composition of the target and laser vaporization/condensation conditions can then be

adjusted to place the system in the region of the phase diagram where the nanowire material is the primary solid phase as the temperature drops towards the solidus line or temperature where the nanocluster solidifies. Hence, it should be possible to exploit this growth framework to yield a wide range of elemental, binary and perhaps more complex 1D nanostructures. We believe that this represents an exciting future opportunity for chemists and materials scientists.

## 3. PHYSICAL PROPERTIES OF NANOTUBES AND NANOWIRES

What are the intrinsic properties of 1D nanostructures and do they exhibit any novel phenomena? The synthetic studies described above have expanded significantly the availability of 1D nanostructures and thus offer great opportunity to study how size and dimensionality affect physical properties. Elucidating the intrinsic properties of nanostructures is, however, an experimentally challenging problem in several respects. First, it is necessary to connect from the outside world to the nanometer scale to enable investigations of, for example, electrical conduction and mechanical deformation. Second, nanostructures prepared by either synthesis or fabrication approaches are not identical objects and typically exhibit dispersions in size and/or structure. Hence, connections to or probes of single nanostructures offer obvious advantages for elucidating their intrinsic physical properties. This point has been demonstrated clearly in several recent studies, including optical investigations of the luminescence from individual CdSe nanoclusters [21] and scanning tunneling microscopy (STM) studies of the atomic structure and local electronic properties of individual single-wall carbon nanotubes [22, 23].

In our work, we have exploited scanned probe microscopies, such as STM and atomic force microscopy (AFM), to interrogate the electrical and mechanical properties of individual 1D nanostructures [5, 22, 24, 25]. Two examples are reviewed below to illustrate the potential of these techniques for defining and uncovering new behavior. These examples focus on the electronic properties of carbon nanotubes and the mechanical properties of nanotubes and nanowires.

### 3.1. *Electronic properties of carbon nanotubes*

The diameter and helicity of a defect free single-walled nanotube (SWNT) [10] are uniquely characterized by the vector $\mathbf{c}_h = n\mathbf{a}_1 + m\mathbf{a}_2 \equiv (n, m)$ that connects crystallographically equivalent sites on a two-dimensional (2D) graphene sheet, where $\mathbf{a}_1$ and $\mathbf{a}_2$ are the graphene lattice vectors and $n$ and $m$ are integers (Fig. 3). Electronic band structure calculations predict that the

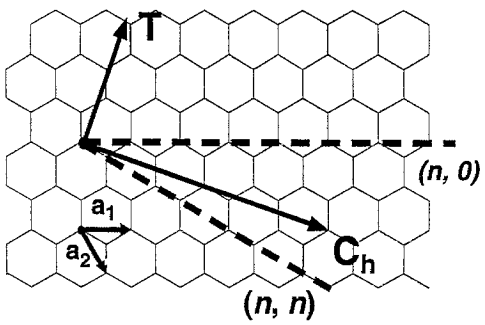


Fig. 3. Schematic of a 2D graphene sheet illustrating lattice vectors $\mathbf{a}_1$ and $\mathbf{a}_2$ and the roll-up vector $\mathbf{c}_h = n\mathbf{a}_1 + m\mathbf{a}_2$. The limiting cases of $(n, 0)$ zigzag and $(n, n)$ armchair tubes are indicated with dashed lines. The nanotube axis is indicated by the vector $\mathbf{T}$.

$(n, m)$ indices determine the metallic or semiconducting behavior of SWNTs [26–28]. Zigzag $(n, 0)$ SWNTs should exhibit two distinct types of behavior: the tubes will be metals when $n/3$ is an integer and otherwise semiconductors. As $\mathbf{c}_h$ rotates away from $(n, 0)$, chiral $(n, m)$ SWNTs are possible with electronic properties similar to the zigzag tubes; that is, when $(2n + m)/3$ is an integer the tubes are metallic and otherwise semiconducting. Finally, when $\mathbf{c}_h$ rotates 30° relative to $(n, 0)$, $n = m$. The $(n, n)$ or armchair tubes are expected to be truly metallic with band crossings at $\mathbf{k} = \pm 2/3$ of the 1D Brilluoin zone. To evaluate this unique behavior (i.e. fundamental changes in electronic properties with subtle variations in structure) requires that the atomic structure and electronic properties of individual tubes be determined; STM represent an ideal tool for obtaining this critical information.

We have carried out STM measurements in ultrahigh vacuum (UHV) at 77 K on purified SWNT samples produced by laser vaporization [22]. Atomically-resolved images were found to exhibit the expected honeycomb lattice as shown in Fig. 4. The chiral angle and diameter for a specific SWNT can be readily determined from such atomic resolution data and thus allow the $(n, m)$ indices of a tube to be defined. From the measured angle and diameter of the tube in Fig. 4(a), it is possible to assign $(n, m)$ indices of either (11, 2) or (12, 2). Note that an (11, 2) tube is expected to be metallic, while a (12, 2) tube should be semiconducting. The SWNT shown in Fig. 4(b) has opposite chirality to that of Fig. 4(a) with indices of (14, −3).

The ability to characterize the electronic properties of the atomically-resolved tubes by tunneling spectroscopy has enabled us to determine whether the electronic properties depend on structure. Specifically, current ($I$) vs voltage ($V$) is measured at specific sites along the SWNTs and differentiated to yield the normalized conductance, $(V/I)\mathrm{d}I/\mathrm{d}V$, which provides a good measure of

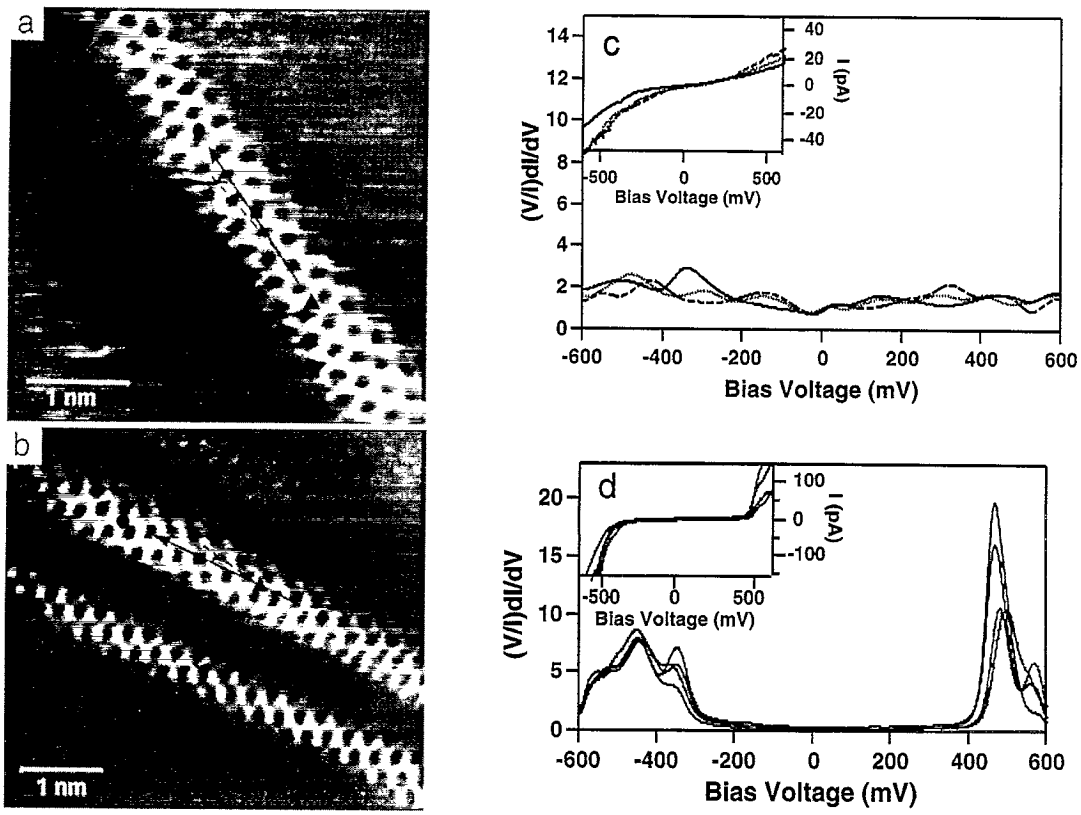


Fig. 4. (a,b) STM images of SWNTs. The solid, black arrows highlight the tube axes and the dashed lines indicate the zigzag direction. The images were recorded in the constant current mode with bias voltages of 50 and 300 mV, respectively, and a tunneling current of 150 pA. The symbols in (a) and (b) correspond to the locations where $I-V$ was measured. (c,d) Calculated normalized conductance, $(V/I)\mathrm{d}I/\mathrm{d}V$ and measured $I-V$ (inset) from the locations indicated in (a,b): –/●; ···/■; – – –/▲; – · ·/◆. Adapted from [22].

the local density of electronic states (LDOS). The LDOS determined for the tube in Fig. 4(a) are roughly constant between −600 and +600 mV as expected for a metal [Fig. 4(c)] and are thus consistent with the (11, 2) indices. Moreover, normalized conductance data recorded on the (14, −3) tube exhibit distinctly different behavior with sharp increases at −325 and +425 mV that correspond to the conduction and valence band edges in the LDOS of a semiconducting tube [Fig. 4(d)].

The characterization of semiconducting and metallic SWNTs with subtle changes in structure have confirmed the remarkable electronic behavior of the nanotubes [22] and we believe represents a significant step forward in understanding these 1D nanostructures. We also believe that this work only scratches the surface of a very rich area. The ability to characterize atomic and electronic structures represents a unique opportunity for testing the level of our understanding of the electronic band structure of these 1D materials; for example, can we obtain quantitative agreement between experiment and theory for the singularities in the DOS vs helicity and diameter and understand the electronic properties of defect and end electronic states? There are also more subtle questions that must be addressed, including (i) does broken rotational symmetry affect the low energy electronic states, (ii) how do coupling to the underlying substrate and mechanical strain perturb the electronic properties and (iii) can signatures of a Luttinger liquid be detected? These represent some of the wide range of future challenges, which if better understood, could serve as the basis for future applications.

### 3.2. *Mechanical properties of nanowires and nanotubes*

Understanding the mechanical properties of nanowires and nanotubes represents another intellectual challenge that could have significant implications for technologies. For example, small whiskers can have strengths considerably greater than those observed in corresponding macroscopic single crystals, an effect attributed to a reduction in the number of defects per unit length (compared with larger structures) that lead to mechanical failure [29]. Systematic increases in strength with decreasing whisker diameters in the 100 to 1 $\mu$m regime clearly supported this idea [30]. It is also true that

the maximum strengths of the best whisker materials fall well below theoretical expectations, and thus it is reasonable to consider whether nanowires and nanotubes can exhibit greater strengths than previously observed in micrometer diameter whiskers. Furthermore, it is worth considering whether such 1D nanostructures can exhibit new phenomena.

To determine directly the mechanical properties of nanowires and nanotubes requires that two connections be made to the material. One of these can be fixed but the other connection must enable displacement and force measurement. Making two connections on such a small scale is inherently difficult; however, in recent studies of the electrical conductivity of carbon nanotubes we devised a flexible method that uses conventional lithography to pin one end of the 1D nanostructure and AFM to locate and probe the regions protruding from the static contact [5, 24]. We have also exploited this same basic approach to measure the mechanical properties as follows [5, 25]. First, nanowires or nanotubes are dispersed randomly on a flat surface and then pinned to this substrate by depositing a regular array of square pads. The AFM is then used to measure directly the lateral force vs displacement (**F–d**) at varying distances from the pinning point as shown in Fig. 5.

The **F–d** curves can be recorded at different positions along the length of the nanowire or nanotube, as the tip is scanned perpendicular to the axis of the beam. After contact, the measured lateral force increases linearly as the beam is elastically deflected from its equilibrium position; the AFM tip remains on the surface during this deflection process. With continued bending it is possible to fracture or plastically deform a nanobeam and thereby determine its strength. Alternatively, the tip can move over the deflected structure when the applied normal load is small, and thus it is possible to deform the beam controllably without damage (Fig. 5). In this way, it has been possible to measure **F–d** curves repeatedly at many points along a 1D nanostructure.

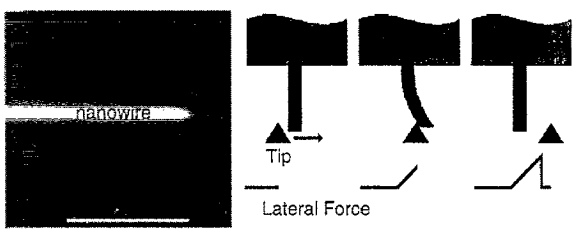


Fig. 5. Overview of the approach used to probe the mechanical properties of nanowires and nanotubes. (left) AFM image of a SiC nanowire that is pinned by a deposited SiO pad at the left side of the image. The scale bar is 500 nm. (right) Schematic of beam bending with an AFM tip. The tip moves in the direction of the arrow while the lateral force is indicated by the bottom trace. Before the tip contacts the 1D nanostructure, the lateral force remains constant and equal to the friction force. After contact, the tip bends the nanostructure and the lateral force increases linearly with displacement. The right most side shows the system after the tip has passed over the 1D nanostructure.

We have previously carried out such measurements on SiC nanowires and carbon nanotubes and have used the resulting data to determine the Young's modulus, strength and toughness of these materials [5, 25]. The **F–d** curves recorded on SiC nanowires and carbon nanotubes showed several important points. First, the initial location at which the lateral **F** increased in each horizontal scan was approximately the same and thus it was possible to conclude that nanowire deflection is elastic. Second, the lateral force recorded in each of the individual scans increased linearly once the tip contacted the nanowire (i.e. $\mathbf{F} = k \cdot \mathbf{d}$) and $k$ decreased for scan lines recorded at increasingly large distances from the pinning point. The Young's modulus (**E**) can be calculated from any given **F–d** curve using $k(x) = (3\pi r^4)/(4x^3)E$, where $x$ is the distance from the pinning point, although we used the full set of curves acquired as a function of position because this provides a more robust determination. From this analysis we found a Young's modulus of 600+/−40 GPa that is in good agreement with the 600 GPa value predicted theoretically for [1 1 1] oriented SiC [25]. Analysis of similar measurements, which were made on multiwall carbon nanotubes with diameters from 26 to 76 nm, yielded a Young's modulus of 1.28+/−0.59 TPa with no dependence on tube diameter. The nanotube modulus is about two times greater than that of our SiC nanowires' and hence one can reasonably claim that nanotubes are the stiffest known material.

Is this the whole story? In fact, the nanotube **F–d** data showed new features that have significant implications

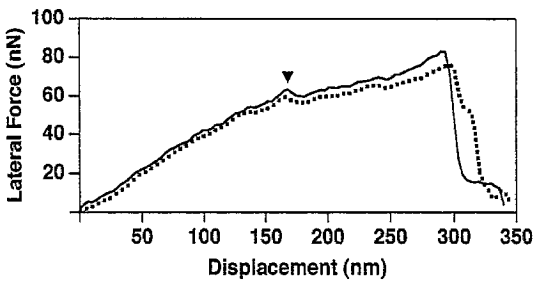


Fig. 6. Two consecutive lateral force traces for a multiwall nanotube. The second, dashed curve was recorded at a distance 2.7 nm down the nanotube from the solid curve. In both traces, the lateral force increases linearly up to the point marked with an inverted black triangle; after this point there is a small drop in restoring force followed by an increase with continued displacement. The large decrease in force at the ends of these traces corresponds to the point at which the tip moves over the nanotube.

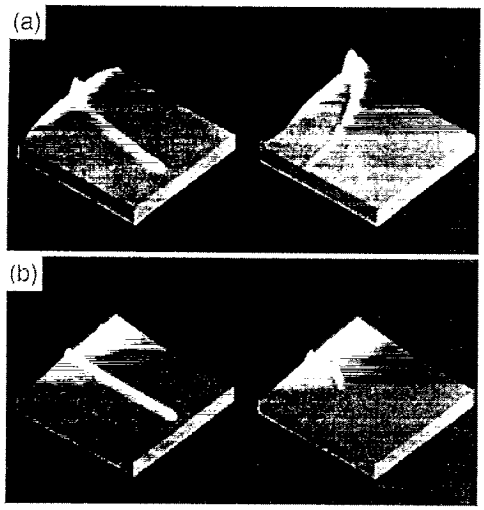


Fig. 7. (a) Images (0.9 $\mu$m by 0.9 $\mu$m) of a 4.4 nm diameter multiwall nanotube before and after bending on an oxidized silicon substrate. The left image shows the nanotube, which was pinned at the left side, in its equilibrium position. The nanotube was then bent by scanning with the tip in contact with the surface. The right image shows bumps along the nanotube that correspond to positions at which buckling occurs. (b) Images (1.25 $\mu$m by 1.25 $\mu$m) of a 21.5 nm diameter SiC nanowire before and after bending on a $MoS_2$ substrate. The left image shows the nanowire, which was pinned at the left side, in its equilibrium position. Application of a high lateral load resulted in the fracture of the nanowire as shown in the right image. Adapted from [25].

for applications. Specifically, the nanotubes can be elastically deflected to a much greater extent than SiC nanowires and the **F–d** curves deviate significantly from the single linear slope predicted for simple beam bending (Fig. 6). The initial linear slope in **F–d** plots decreases abruptly when the nanotubes are deflected by relatively large amounts. The similarity of adjacent **F–d** curves strongly suggests, however, that the abrupt change in slope corresponds to an elastic process. This behavior deviates from that reported in previous mechanical deflection studies of whiskers [30] and that found for our SiC nanowires, although it does agree qualitatively with recent simulations suggesting that nanotubes buckle elastically to yield a structure reminiscent of that formed when a macroscopic rubber tube is bent and kinked [31]. Further evidence supporting this conclusion was obtained in direct bending experiments in which high friction substrates were used to trap nanotubes in highly deflected configurations (Fig. 7). Significantly, these images showed a bead-like structure that is consistent with the expected height increases at the buckling points [25].

The large **E**'s determined for carbon nanotubes and SiC nanowires make these materials obvious candidates for the reinforcing elements in composites. Although many factors must be considered in making a useful composite, at least the strength and toughness of the reinforcing material must be quantified, since they place limits on the potential composite properties. Strength and toughness refer, respectively, to the maximum force per unit area and the elastic energy stored or absorbed by a material before failure. The bending strength for SiC nanowires is determined from the maximum strain (at the pinning site) just prior to fracture (Fig. 7) and for the nanotubes the bending strength is defined to be the strain determined at the initial buckling point [25]. The average bending strength determined for nanotubes was found to be 14.2+/−8.0 GPa. In contrast, the largest SiC nanowire strength observed, 53.4 GPa, is significantly larger than the nanotube values and approaches the predicted maximum of 0.1**E**. This nanowire strength value is also a factor of 2 times the best observed previously in micrometer diameter SiC whiskers. Hence, these strength results indicate that SiC nanowires, despite their smaller **E**, should be a better reinforcing material in some composite structures than carbon nanotubes. Carbon nanotubes should, however, be considered for other types of mechanical applications. In particular, the elastic buckling exhibited by carbon nanotubes makes then exceedingly tough materials. Hence, the ability of carbon nanotubes to sustain elastically loads at large deflection angles enables them to store or absorb considerable energy. One obvious application of this unique energy absorbing capability of carbon nanotubes would be in armor, although a suitable matrix would be needed to exploit these properties in a bulk material.

These measurements of the intrinsic mechanical properties begin to provide justification for speculation that 1D nanostructures have great potential in mechanical applications. We still believe that there is much to be learned at the basic level; for example, how does the modulus and strength scale with size for sub 10 nm diameter structures and can a method be devised to measure the intrinsic tensile strength of these materials? Answers to these and other questions represent an exciting challenge for the future.

## 4. APPLICATIONS: NANOPROBES AND NANOSTRUCTURED MATERIALS

The basic studies discussed above review some of the exciting advances being made in understanding how to assemble rationally nanowires and to probe their intrinsic physical properties. This discussion also made clear how little we understand and the many opportunities for fundamental research in the future. In this regard, it is reasonable to ask whether we now know enough about the growth and properties of 1D nanostructures to

consider potential applications. We argue below that in some cases the answer to this question is yes, and illustrate this answer briefly with two very different examples: the use of carbon nanotubes as tips for AFM and the use of nanowires to create nanostructured superconductors with high critical current densities.

### 4.1. *Novel probes for AFM*

The feature resolution obtained by AFM is determined in large part by the size and shape of the probe tip used for imaging [32, 33]. Commercially available probes consist of microfabricated pyramids of Si or $Si_3N_4$ that have end radii of curvature as small as 10 nm but are often much larger [33]. These tips place significant constraints on potential lateral resolution and furthermore, the pyramidal shape restricts the ability of these tips to access narrow and deep features. Recently, a potential breakthrough in probe technology was achieved by attaching multiwall carbon nanotubes to the ends of Si tips [34]. The high aspect ratio nanotube tips have obvious advantages for probing deep crevices and steep features and were exploited for this purpose by Dai *et al.* [34]. Additionally, the ability of nanotubes to elastically buckle [25], as described above, limits the maximum force applied to a sample, which can prevent damage to delicate organic and biological samples and at the same time makes the tips very robust.

We have also shown recently that carbon nanotubes can provide significantly improved lateral resolution [35]. A typical scanning electron microscopy image of a tip attached to a conventional single-crystal silicon cantilever-tip assembly is shown in Fig. 8. To explore the resolution of these tips and their applicability to high-resolution imaging of biological samples we have investigated amyloid-$\beta$ 1-40 ($A\beta 40$) fibrils produced *in vitro*. $A\beta$ fibrils are the primary constituent of the insoluble core of amyloid plaques that are characteristic of Alzheimer's disease and thus represents a significant scientific problem to attack.

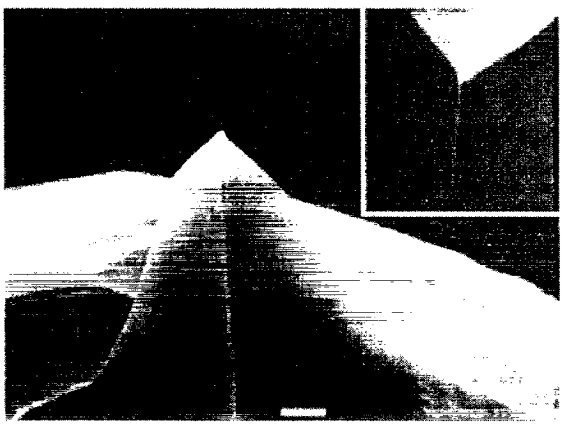

Fig. 8. SEM image of a multiwall nanotube tip attached to a silicon cantilever-tip assembly. The inset corresponds to a higher magnification view that highlights the nanotube. The orientation of the inset is rotated 180° relative to the main image. The white bar corresponds to 1 $\mu$m. Adapted from [35].

The sizes of nanotube tips have been determined by deconvoluting the tip radii from the observed fibril widths [35]. On average this type of analysis has shown that the multiwall nanotube tips exhibit radii of 9 nm compared with 13–20 nm for Si. Even more impressive have been the results obtained with SWNTs that show an average effective radius of only 3 nm [35]. We believe that the use of SWNT tips is especially promising, since the observed radii are still substantially larger than the 0.5–0.7 nm radii of individual SWNTs. These studies have demonstrated that significantly improved lateral resolution is attainable on biological samples using multiwall nanotube and SWNT probe tips. While further improvements in resolution will be needed in order to approach true molecular resolution imaging in air and in liquids, nanotube tips offer a rational pathway to do so in the future. Moreover, nanotube tips can be covalently functionalized at their ends to create chemically and biologically sensitive probes [36]. In the future, we believe that this "application" provides a significant challenge for basic science with a very big payoff: a chemically-sensitive, molecular resolution probe for soft condensed matter systems.

### 4.2. *Nanostructured materials*

With our emerging understanding of both synthetic methods and physical properties of 1D nanostructures, we have also begun to explore the possibility of exploiting these materials for developing nanostructured solids. A particularly exciting example of this work is the development of high critical current density ($J_c$), high-temperature superconductors (HTS) [37–39]. Large $J_c$ are essential to many proposed applications of the HTSs such as wires for power transmission cables and solenoids. In general, $J_c$ is limited by two major factors, including thermally activated flux motion and poor alignment of superconducting grains. Thermally-activated flux flow is an intrinsic limitation and arises from the short coherence lengths and large anisotropy of the HTS materials that leads to a weak pinning of flux-lines [40, 41].

Theoretical and experimental studies have shown, however, that this intrinsic problem in HTSs can be reduced significantly by creating correlated defects, such as columnar defects, in the crystal lattice [42, 43]. Indeed, the large enhancement of $J_c$ produced by columnar defect structures argues that chemical (vs physical) strategies should be considered for their creation in HTS materials. For example, the incorporation

of 1D nanostructures into a HTS matrix should yield the same beneficial effect as ion-generated columnar defects. Indeed, we have shown that MgO nanowires can be incorporated into $Bi_2Sr_2Ca_{n-1}Cu_nO_{2n+4}$ (BSCCO) and other HTS materials to form nanostructured composites [37–39]. The columnar defect structure in the nanowire/BSCCO composites was clearly shown in electron microscopy images. Moreover, systematic TEM analysis of the nanowire orientation in HTS composites has shown that there are two preferred orientations: parallel and perpendicular to the *c*-axis; that is, the nanowires are not oriented isotropically in these samples. We have suggested that the preferred orientation or self-organization of the MgO nanowires after melt-texturing occurs because the exposed MgO surfaces are lattice-matched substrates for the growth of BSCCO with either the *a/b* or *c*-axes oriented perpendicular to the nanowire axis. Hence, the synthesis of MgO nanowires serves a dual purpose: (i) this oxide minimizes deleterious reactions with the HTS matrix and (ii) the structure leads to self-organization within BSCCO. Because oriented columnar defects are expected to produce improved $J_c$ compared to an isotropic distribution, we believe that the observed self-orientation of MgO nanowires during composite processing is significant for applications. More generally, our concept of self-organization, which is driven by lattice epitaxy, will be an important one to exploit in the future as we explore the synthesis of other nanostructured materials.

We have also characterized systematically $J_c$ in the nanowire/HTS composites and HTS reference samples as a function of magnetic field ($H$) and temperature ($T$) [37–39]. In general, the nanowire/HTS composites exhibit large increases in $J_c$ compared to the reference samples and these increases are especially significant at higher $H$ and $T$. The enhancements in $J_c$ and shift of the irreversibility line found in nanowire/BSCCO composites are comparable to those observed previously in ion-irradiated samples [43, 44]. The maximum density of nanowire defects we have achieved, however, corresponds to an effective field of 0.25 T that is lower than achieved by irradiation. Nevertheless, we believe that the ability to make samples with strong-pinning columnar defects by a rational nanochemistry approach has distinct advantages over irradiation with GeV protons for large scale applications. The development of these and other functional, nanostructured solids promises to be an exciting and challenging area of nanoscale chemistry in the future.

*Acknowledgements*—C.M.L. graciously acknowledges the students and postdoctoral fellows who have carried out the work described in this review, including J. Hu, J.-L. Huang, P. Kim, A. Morales, T.W. Odom, P.E. Sheehan, E.W. Wong and P. Yang. I would also like to thank the National Science Foundation, Office of Naval Research and Air Force Office of Scientific Research for their generous financial support.

## REFERENCES

1. *Nanostructures and Mesoscopic Systems* (Edited by M.A. Reed and W. Kirk). Academic, San Diego, 1992.
2. Alivisatos, A.P., *Science*, **271,** 1996, 933.
3. Dvoret, M.H., Esteve, D. and Urbina, C., *Nature*, **360,** 1992, 547.
4. Ashoori, R.C., *Nature*, **379,** 1996, 413.
5. Lieber, C.M., Morales, A.M., Sheehan, P.E., Wong, E.W. and Yang, P., in *Proceedings of the Robert A. Welch Foundation 40th Conference on Chemical Research: Chemistry on the Nanometer Scale*, p. 165. R.A. Welch Foundation, Houston, 1997.
6. Murray, C.B., Kagan, C.R. and Bawendi, M.G., *Science*, **270,** 1995, 1335.
7. Voit, J., *Rep. Prog. Phys.*, **57,** 1994, 977.
8. Kane, C., Balents, L. and Fisher, M.P.A., *Phys. Rev. Lett.*, **79,** 1997, 5086.
9. Colbert, D.T., Zhang, J., McClure, S.M., Nikolaev, P., Chen, Z., Hafner, J.H., Owens, D.W., Kotula, P.G., Carter, C.B., Weaver, J.H., Rinzler, A.G. and Smalley, R.E., *Science*, **266,** 1994, 1218.
10. Thess, A., Lee, R., Nikolaev, P., Dai, H., Petit, P., Robert, J., Xu, C., Lee, Y.H., Kim, S.G., Rinzler, A.G., Colbert, D.T., Scuseria, G.E., Tomanek, D., Fischer, J.E. and Smalley, R.E., *Science*, **273,** 1996, 483.
11. Martin, C.R., *Science*, **266,** 1994, 1961.
12. Wu, C.-G. and Bein, T., *Science*, **266,** 1994, 1013.
13. Dai, H., Wong, E.W., Lu, Y.Z., Fan, S. and Lieber, C.M., *Nature*, **375,** 1995, 769.
14. Wagner, R.S. and Ellis, W.C., *Appl. Phys. Lett.*, **4,** 1964, 89.
15. Wagner, R.S., in *Whisker Technology* (Edited by A.P. Levitt), p. 47. Wiley, New York, 1970.
16. Dietz, T., Duncan, M., Liverman, M. and Smalley, R.E., *J. Chem. Phys.*, **73,** 1980, 4816.
17. Morales, A.M. and Lieber, C.M., *Science*, **279,** 1998, 208.
18. Goldstein, A.N., Echer, C.M. and Alivisatos, A.P., *Science*, **256,** 1992, 1425.
19. Hu, J., Duan, X. and Lieber, C.M., *Adv. Mater.*, submitted for publication.
20. Westwater, J., Gosain, D.P., Tomiya, S., Usui, S. and Ruda, H., *J. Vac. Sci. Technol.*, **B15,** 1997, 554.
21. Empedocles, S.A., Norris, D.J. and Bawendi, M.G., *Phys. Rev. Lett.*, **77,** 1996, 3873.
22. Odom, T.W., Huang, J.-L., Kim, P. and Lieber, C.M., *Nature*, **391,** 1998, 62.
23. Wildoer, J.W.G., Venema, L.C., Rinzler, A.G., Smalley, R.E. and Dekker, C., *Nature*, **391,** 1998, 59.
24. Dai, H., Wong, E.W. and Lieber, C.M., *Science*, **272,** 1996, 523.
25. Wong, E.W., Sheehan, P.E. and Lieber, C.M., *Science*, **277,** 1997, 1971.

26. Mintmire, J.W., Dunlap, B.I. and White, C.T., *Phys. Rev. Lett.*, **68,** 1992, 631.
27. Hamada, N., Sawada, S. and Oshiyama, A., *Phys. Rev. Lett.*, **68,** 1992, 1579.
28. Saito, R., Fujita, M., Dresselhaus, G. and Dresselhaus, M.S., *Appl. Phys. Lett.*, **60,** 1992, 2204.
29. Levitt, A.P., in *Whisker Technology* (Edited by A.P. Levitt), p. 1. Wiley, New York, 1970.
30. Mehan, R.L. and Herzog, J.A., in *Whisker Technology* (Edited by A.P. Levitt), p. 157. Wiley, New York, 1970.
31. Yakobson, B.I., Brabec, C.J. and Bernholc, J., *Phys. Rev. Lett.*, **76,** 1996, 2511.
32. Noy, A., Vezenov, D. and Lieber, C.M., *Annu. Rev. Mater. Sci.*, **27,** 1997, 381.
33. Shao, Z. and Yang, J., *Quart. Rev. Biophys.*, **28,** 1995, 195.
34. Dai, H., Hafner, J.H., Rinzler, A.G., Colbert, D.T. and Smalley, R.E., *Nature*, **384,** 1996, 147.
35. Wong, S.S., Harper, J.D., Lansbury, P.T. and Lieber, C.M., *J. Am. Chem. Soc.*, **120,** 1998, 603.
36. Wong, S.S., Joselevich, E., Woolley, A.T., Cheung, C.L. and Lieber, C.M., *Nature*, in press.
37. Yang, P. and Lieber, C.M., *Science*, **273,** 1996, 1836.
38. Yang, P. and Lieber, C.M., *Appl. Phys. Lett.*, **70,** 1997, 3158.
39. Yang, P. and Lieber, C.M., *J. Mater. Res.*, **12,** 1997, 2981.
40. Pashitski, A.E., Polyanskii, A., Gurevich, A., Parrell, J.A. and Larbalestier, D.C., *Physica*, **C246,** 1995, 133.
41. Bishop, D.J., Gammel, P.L., Huse, D.A. and Murray, C.A., *Science*, **255,** 1992, 165.
42. Nelson, D.R. and Vinokur, V.M., *Phys. Rev. Lett.*, **68,** 1992, 2398.
43. Kummeth, P., Struller, C., Neumuller, H.-W. and Saemann-Ischenko, G., *Appl. Phys. Lett.*, **65,** 1994, 1302.
44. Krusin-Elbaum, L., Thompson, J.R., Wheeler, R., Marwick, A.D., Li, C., Patel, S., Shaw, D.T., Lisowski, P. and Ullmann, J., *Appl. Phys. Lett.*, **64,** 1994, 3331.